PELVIS

Image quality and diagnostic accuracy of complex-averaged high b value images in diffusion-weighted MRI of prostate cancer

Hamed Kordbacheh[2] · Ravi Teja Seethamraju[5] · Elisabeth Weiland[3] · Berthold Kiefer[3] · Marcel Dominik Nickel[3] ·
Thitinan Chulroek[2,4] · Martina Cecconi[2] · Vinit Baliyan[2] · Mukesh G. Harisinghani[1,2]

Abstract

Purpose To evaluate the impact of complex-averaging on image quality (IQ) and diagnostic accuracy of acquired and calculated high b value (aHBV, cHBV) images in diffusion-weighted prostate MRI.

Materials and methods This retrospective study included 84 patients who underwent multiparametric prostate MRI at 3 Tesla without endorectal coil. DWIs were acquired at three different b values which included two lower b values ($b = 50,900$ s/mm^2) and one higher b value (aHBV at 2000 s/mm^2). The acquired data were postprocessed to generate two different types of trace-weighted images—using conventional magnitude-averaging and complex-averaging. Using lower b values ($b = 50,900$ s/mm^2) from both conventional and complex-averaged image sets, cHBV images ($b = 2000$ s/mm^2) and ADC maps were derived. All image sets were reviewed by two radiologists in different reading sessions to assess image quality and PIRADS. The diagnostic accuracy of different image sets for the detection of prostate lesions was performed by correlating PIRADS and Gleason scores.

Results Complex-averaging did not impact ADC values of the prostate lesions compared to magnitude-averaging ($P = 0.08$). Complex-averaging improved image quality of acquired high b value and calculated high b value images ($P < 0.0001$). Complex-averaging also improved the level of confidence (LOC) of the acquired high b value for both readers ($P < 0.0001$, $P < 0.05$), but only for reader A in calculated high b value ($P < 0.0001$). The image quality of calculated high b value images was not significantly different than acquired high b value images. The dataset combining complex-averaging and calculated high b value provided the highest diagnostic accuracy (but not statistically significant) for detection of the significant prostate lesion compared to the magnitude-averaged acquired high b value (79.55% vs. 72.73%; $P = 0.317$). The mean acquisition time for $b = 2000$ s/mm^2 sequence (aHBV) was 6 min 30 s (± 1 min 16 s) out of a total of 28 min 31 s (± 4 min 26 s) for the entire mp-MRI protocol (approximately 25% of total scan time).

Conclusion Complex-averaging provides better image quality and level of confidence without significant impact on ADC values and diagnostic accuracy for detection of the significant prostate lesions . The calculated high b value images are also comparable to (and can substitute) the acquired high b value images which can help in reducing the imaging time.

Keywords Image quality · Multiparametric MRI · Prostate cancer

Introduction

Prostate cancer is the most common newly diagnosed cancer among men in the western world and the second-most common disease worldwide [1]. Not only does multiparametric (mp)-MRI prior to biopsy may help in avoiding unnecessary biopsies in 30% of patients, but it may also reduce the rate

of over diagnosis and overtreatment due to a detection bias of MRI toward significant disease [2]. Diffusion-weighted MRI (DW-MRI) has emerged as a key MRI technique for the detection of significant prostate cancer [3–5]. High b value images are particularly useful for diffusion weighting as they provide better tissue contrast and less T2 shine-through effect [6, 7] and thereby help differentiate benign from malignant prostate lesions. However, their acquisition contributes significantly to the total scan time in mp-MRI [8–10], and they also suffer from the decreased signal-to-noise ratio (SNR), susceptibility effects, and distortions [6,

✉ Mukesh G. Harisinghani
mharisinghani@mgh.harvard.edu

Extended author information available on the last page of the article

11, 12]. Extrapolated calculated high b value images is a strategy to avoid these effects and to reduce the total scan time [8, 13–17].

There are new technical advances to address the challenges of high b value DWI, and complex-averaging is one of these. Due to inherent low SNR in particular at high b values, diffusion images with same contrast are acquired multiple times and then averaged. As DWI is also very sensitive to phase variations, this is conventionally done by taking the magnitude first. This approach is very robust, but also changes the noise distribution which is no longer centric. Consequently, the average has a noise bias that appears as a haze-like background in low signal regions. This can be circumvented by an adaptive combination of complex-valued images (complex-averaging) [18]. With this approach, local phase variations between different images are implicitly aligned, and therefore, the combined image no longer has a noise bias. This improves image appearance and SNR in low signal regions. Some of the prior studies [8, 13–17] have evaluated the performance of acquired and calculated high b value images with variable results, but complex-averaging is a relatively new method which can be used with acquired and calculated datasets and has not been previously tested. The purpose of this study was to assess the impact of complex-averaging on image quality and diagnostic accuracy of acquired and calculated high b value (aHBV, cHBV) images in patients with prostate cancer.

Materials and methods

Patient cohort and study design

Institutional Review Board (IRB) and Health Insurance Portability and Accountability Act (HIPAA) approval were obtained, and the requirement for informed consent was waived by our hospital IRB. In this retrospective study, we included eighty-four consecutive patients who underwent multiparametric prostate MRI on a MAGNETOM Skyra 3T system (Siemens Healthcare, Erlangen, Germany) using 18-channel body matrix and 32-channel spine matrix coils between January 2017 and December 2017. These patients underwent prostate MRI because of elevated prostate-specific antigen level and/or suspicion of prostate cancer at digital rectal examination (before biopsy).

Multiparametric MR protocol and parameters

At our institution, mp-MRI of the prostate typically includes T2-weighted images in 3 orientations, axial diffusion-weighted imaging (DWI) with multiple b values of $b = 50$ s/mm^2 and 900 s/mm^2 from which an ADC map and a calculated high b value image is derived, a separately acquired,

axial high b value image with $b = 2000$ s/mm^2 and axial dynamic contrast-enhanced (DCE) imaging acquired over 2 min. DWI was performed using a prototype sequence that essentially differs from the product sequence by the outlined scanner integrated postprocessing. Sequence parameters of the diffusion protocols can be found in Table 1. All scans are acquired with a slice thickness of 3 mm.

Calculated diffusion-weighted images

As discussed above, the high b value can be derived/calculated from the acquired lower b value images in order to improve SNR and avoid susceptibility effects and distortions [6, 8, 11–13]. Fitting the acquired b value images to a mono-exponential signal model for determining the T2-weighted magnetization M_0 and the apparent diffusion coefficient (ADC) allows extrapolating to diffusion-weighted images at arbitrary b values. Of interest are very high b value images and regions with restricted diffusion, such as tumors, that will stand out and allow an easy visual detection. For prostate cancer, the contrast of $b = 2000$ s/mm^2 is often chosen, and here derived two lower b values ($b = 50$, 900 s/mm^2) using the above-mentioned mono-exponential model.

The approach of cHBV images works well in regions with well determined M_0, but artificially enhances noise in regions with low M_0 and low ADC values. This may be irrelevant for the target region but leads to irritating background in the extrapolated high b value images. To address this issue in a manner that does not modify the extrapolated b values in actual region of interest, but still addresses the issue of artificial signal enhancement, the following steps were performed: (1) A noise level was determined based on all pixels with a determined ADC smaller than 300 μm^2/s. (2) For pixel with a T2-weighted magnetization below the determined noise level, the ADC value used for

Table 1 Diffusion sequence parameters

	cHBV	aHBV
b values (averages) (s/mm^2)	50 (2)/900 (9)	2000 (15)
Calculated b value (s/mm^2)	2000	n.a.
Diffusion mode	4-Scan Trace	4-Scan Trace
FOV (mm)	220×220	220×220
Matrix	114×114	114×114
Slice thickness (mm)	3	3
Number of slices	18 to 36 (depending on the gland size)	18 to 36 (depending on the gland size)
TE (ms)	67	75
TR (ms)	3700	4900
TA (20 slices) (min)	2:55	5:20
FatSat mode	FatSat	FatSat

extrapolating diffusion-weighted images above the highest acquired b value was set to a minimal ADC value that gradually increased from 0 to 1000 $\mu m^2/s$ for M_0 decreasing from the noise level to zero.

Complex-averaging of diffusion-weighted images

With the phase of complex-valued diffusion-weighted images being very sensitive to confounding factors such as bulk motion, it is established to perform pixelwise averaging of repeated measurements with identical diffusion encoding based on magnitude values. The approach is robust but comes at the cost that noise no longer cancels out completely in the averaged images and leads to a haze-like background and resultant low SNR. The issue can be circumvented by an adaptive combination of complex-valued images, like the approach taken for the combination of received coil images [18]. Here, a combination of images in local patches is performed without explicitly performing a phase correction of the single images. Referring to Ref. [18] for more technical details, the method is suited for the combination of images that are expected to have the same pixelwise magnitude but are subject to individual signal variations that are of lower resolution and that can be complex-valued. In case of phased-array coils as discussed in [18], these variations correspond to coil sensitivity maps. In the present work, these are the phase variations of the individual averages, e.g., due to bulk motion. The approach assumes that the individual phase variations can be assumed as constant in local patches of the images. In this work, the patch size was chosen to be 7×7 pixels. An important advantage of this approach compared to conventional phase correction is that the relative weight of each image in the combination is additionally determined locally for each patch.

Image evaluation

Qualitative evaluation of the calculated and acquired high b value DWI images datasets for both complex-averaged and regular datasets was performed by two radiologists (8 and 10 years of experience) on a PACS workstation (AGFA Impax; AGFA Technical Imaging Systems, Ridgefield Park, NJ) in separate reading sessions with intervals of 3 weeks. The radiologists assessed the image quality (IQ), and level of confidence (LOC). A 3-point scale was used for image quality parameters including: noise, artifact, and resolution (3-good quality for diagnostic interpretation, 2-moderate quality for diagnostic interpretation, 1-poor quality for diagnostic interpretation). Level of confidence was rated on a scale of 1 to 5 ($1 \leq 25\%$, $2 = 25$–50%, $3 = 50$–75%, $4 = 75$–90%, $5 \geq 90\%$) [19]. They also performed PIRADS score in consensus for detected lesions in each session while they were blinded to the clinical details. DWI sequences were of key importance

for the final PI-RADS score if the tumor was in the peripheral zone and T2W images in the transitional zone [20, 21]. For all detected lesions, ADC measurement (free-hand ROI drawn over the entire lesion) was performed by a single observer from both magnitude-averaged and complex-averaged datasets in two separate reading sessions but on similar workstations.

For the reading session, MR scans were organized in four sets of images: Image set 1 to set 4.

Image set 1 consisted of (a) axial T1-weighted and axial, sagittal, and coronal T2-weighted images; (b) axial acquired magnitude-averaged high b value images (including the corresponding ADC maps).

Image set 2 consisted of (a) axial T1-weighted and axial, sagittal, and coronal T2-weighted images; (b) axial acquired complex-averaged high b value images (including the corresponding ADC maps).

Image set 3 consisted of (a) axial T1-weighted and axial, sagittal, and coronal T2-weighted images; (b) axial calculated magnitude-averaged high b value images (including the corresponding ADC maps).

Image set 4 consisted of (a) axial T1-weighted and axial, sagittal, and coronal T2-weighted images; (b) axial calculated complex-averaged high b value images (including the corresponding ADC maps).

The electronic medical records of every patient were then reviewed to document patient demographics, PSA level, biopsy result, and clinical diagnosis. For lesions with histological confirmation ($n = 46$), the correlation was performed between consensus PIRADS and Gleason scores. A Gleason score ≥ 7 were considered as the presence of significant prostate cancer. Diagnostic performances regarding sensitivity, specificity, positive predictive value, negative predictive value, and accuracy were calculated for all the image datasets. In detail, regarding the accuracy for the detection of significant prostate cancer, PI-RADS v2 scores of 1–2–3 were considered negative, and PI-RADS v2 scores of 4–5 were considered positive. To make sure that the histopathology reflected the reported lesion on MRI, the lesion site and biopsy site descriptors (right vs left; base vs. mid-gland vs. apex) were matched.

Statistical analysis

Microsoft Excel 2007 (Microsoft Corporation) and MedCalc software (Version 18.2.1, Ostend, Belgium) were used for statistical analyses. Group statistics were presented as mean $\pm$ SD, numbers, and percentages. The comparisons were made using Wilcoxon test and McNemar's test. P values less than 0.05 were considered as statistically significant.

Results

Patient cohort

The final patient cohort included 84 patients between January 2017 and December 2017. The average age in this patient cohort was 64 ± 8 years (range 45–84 year). The mean PSA was 10.35 ± 15.53 ng/ml. Prostate biopsy report or prostatectomy operation note was available for 46 patients. In 11 cases, prostatectomy operation note was used as the reference, and in 35 cases, we used standard 12-core biopsy/guided biopsy report to determine the Gleason score. The mean scan time for the mp-MRIs was 28 min 31 s (± 4 min 26 s) and for $b = 2000$ s/mm² sequence was 6-min 30 s (± 1 min 16 s). The aHBV protocol accounted for approximately 25% of total scan time.

Image evaluation

Qualitative analysis

Complex-averaging improved Image Quality of the acquired and calculated high b value DWI for both readers ($P < 0.0001$) (Figs. 1, 2). Mean image quality of the complex-averaged acquired high b value DWI for reader A and B was 2.67 and 2.69, respectively, which was significantly higher than conventional magnitude-averaged acquired high b value DWI for both readers (1.81 and 2.10, respectively) ($P < 0.0001$). Mean image quality of the Complex-averaged calculated high b value DWI for reader A and B was 2.70 and 2.64, respectively which was significantly higher than conventional magnitude-averaged calculated high b value DWI for both readers (1.92 and 2.25, respectively) ($P < 0.0001$) (Fig. 1; Table 2). Complex-averaging improved LOC of the aHBV for both readers ($P < 0.0001$, $P < 0.05$). Mean LOC of the complex-averaged acquired high b value DWI for readers A and B was 4.10 and 4.37, respectively which was significantly higher than conventional magnitude-averaged acquired high b value DWI for both readers (3.01 [$P < 0.0001$] and 4.06 [$P < 0.05$], respectively). Mean LOC of the complex-averaged calculated high b value DWI for reader A was significantly higher than conventional magnitude-averaged calculated high b value DWI (4.24 vs. 3.32, [$P < 0.0001$]). Mean LOC of the complex-averaged calculated high b value DWI for reader B was higher but not statistically significant than conventional magnitude-averaged calculated high b value DWI (4.35 vs. 4.10, [$P = 0.058$]) (Table 2).

The IQ values of the cHBV were not significantly different than aHBV images for both readers (Fig. 3). The LOC of the conventional magnitude-averaged cHBV was significantly higher than conventional magnitude-averaged aHBV images for reader A (3.32 vs. 3.01, $P = 0.02$) but was not significant for reader B (4.1 vs. 4.06, $P = 0.38$). The LOC of the complex-averaged cHBV images were not significantly different than Complex-averaged aHBV images for both readers ($P = 0.2$ and 0.43) (Table 3).

Complex-averaging did not impact ADC values of the prostate lesions compared to magnitude-averaging ($P = 0.08$). Mean of the ADC values of the lesions was $934 \pm 241 \times 10^{-6}$ mm²/s (range $531–1433 \times 10^{-6}$ mm²/s) from complex-averaged ADC maps, which was not significantly different from the mean of the ADC values of the lesions from conventional magnitude-averaged ADC maps
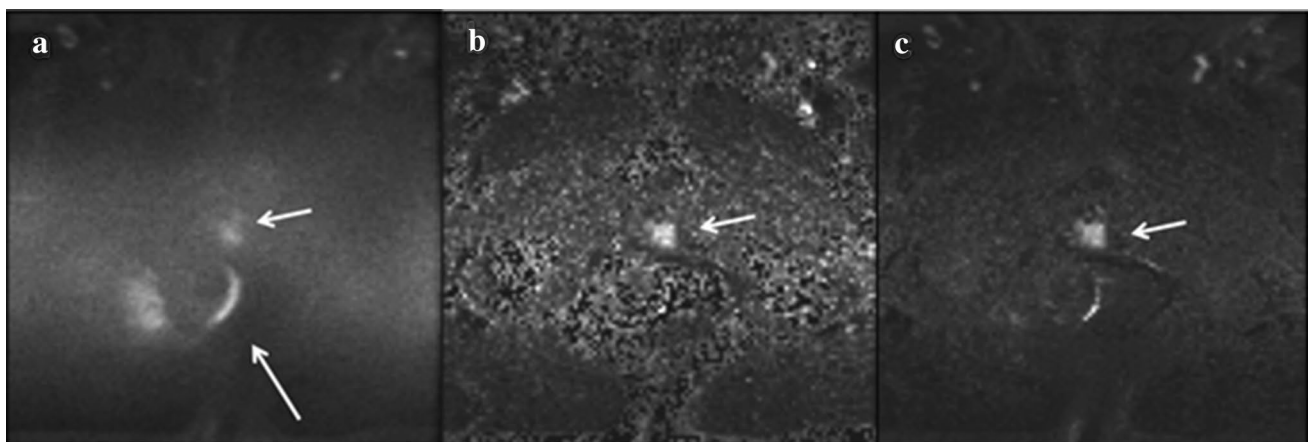

Fig. 1 A 74-year-old man with clinically significant prostate cancer (Gleason score 7 from prostatectomy, PSA = 9.83 ng/ml). Acquired magnitude-averaged $b = 2000$ s/mm² images **a** are prone to susceptibility effects and distortion (from rectal gas in this case; long arrow). Calculated $b = 2000$ s/mm² images **b** show lesser image distortion and susceptibility effects. The combination of the calculated high b value and complex-averaging **c** further improves the image quality
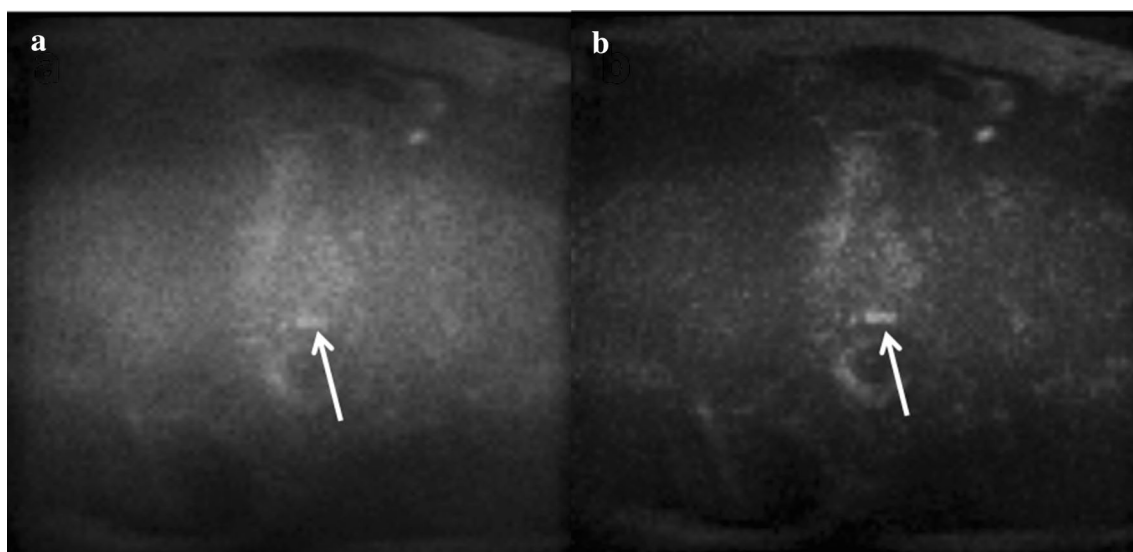
Fig. 2 A 60-year-old man with Gleason score 6 prostate lesion from prostatectomy, and PSA = 3.36 ng/ml. Magnitude-averaged $b = 2000$ s/mm^2 images **a** demonstrate a background signal build up resulting in a haze and lower signal-to-noise ratio. This can be resolved using complex-averaged images **b**, which have relatively higher signal-to-noise ratio. The resolution of the background haze also results in better conspicuity of focal lesions with diffusion restriction (**b**)

Table 2 Comparing image quality and level of confidence between magnitude-averaged and complex-averaged high b value images

	Reviewer A	Reviewer B
Image quality		
Acquired complex-averaged high b value	2.67	2.69
Acquired magnitude-averaged high b value	1.81	2.10
P value*	< 0.0001	< 0.0001
Calculated complex-averaged high b value	2.70	2.64
Calculated magnitude-averaged high b value	1.92	2.25
P value*	< 0.0001	< 0.0001
Level of confidence		
Acquired complex-averaged high b value	4.10	4.37
Acquired magnitude-averaged high b value	3.01	4.06
P value*	< 0.0001	< 0.05
Calculated complex-averaged high b value	4.24	4.35
Calculated magnitude-averaged high b value	3.32	4.10
P value*	< 0.0001	0.058

*Mann–Whitney test was used for comparisons

$(920 \pm 241 \times 10^{-6}$ mm^2/s; range $501-1457 \times 10^{-6}$ mm^2/s$)$ $(P = 0.08)$.

Lesion visibility and PIRADS score

The combination of complex-averaging and cHBV provided the highest diagnostic accuracy for detection of the clinically significant lesion (Gleason score ≥ 7) (Table 4). The specificity of calculated HBV was higher than the acquired HBV in detecting the clinically significant prostate lesion (88% vs. 80%; for both magnitude- and complex-averaged). The sensitivity of complex-averaged DW images was higher than that of the conventional magnitude-averaged DW images in both the acquired and calculated DWI (68.4% vs. 63.1% in calculated DWI and 73.6% vs. 63.1% in acquired DWI). The accuracy of complex-averaged DW images was higher than the conventional magnitude-averaged DW images in both acquired and calculated DWI (79.5% vs. 77.2% in calculated DWI and 77.2% vs. 72.7% in acquired DWI) (Table 4).

Discussion

We are presenting results with the use of a novel complex-averaging method and its impact on image quality and diagnostic accuracy of high b value images in diffusion-weighted MRI of prostate cancer. Our findings suggest that complex-averaging improves the image quality and results in higher level of confidence without having any effect on the quantitative information in the ADC maps. In addition, complex-averaging provides comparable diagnostic accuracy of DWI for the clinically significant prostate cancer. We also assessed the performance and quality of calculated
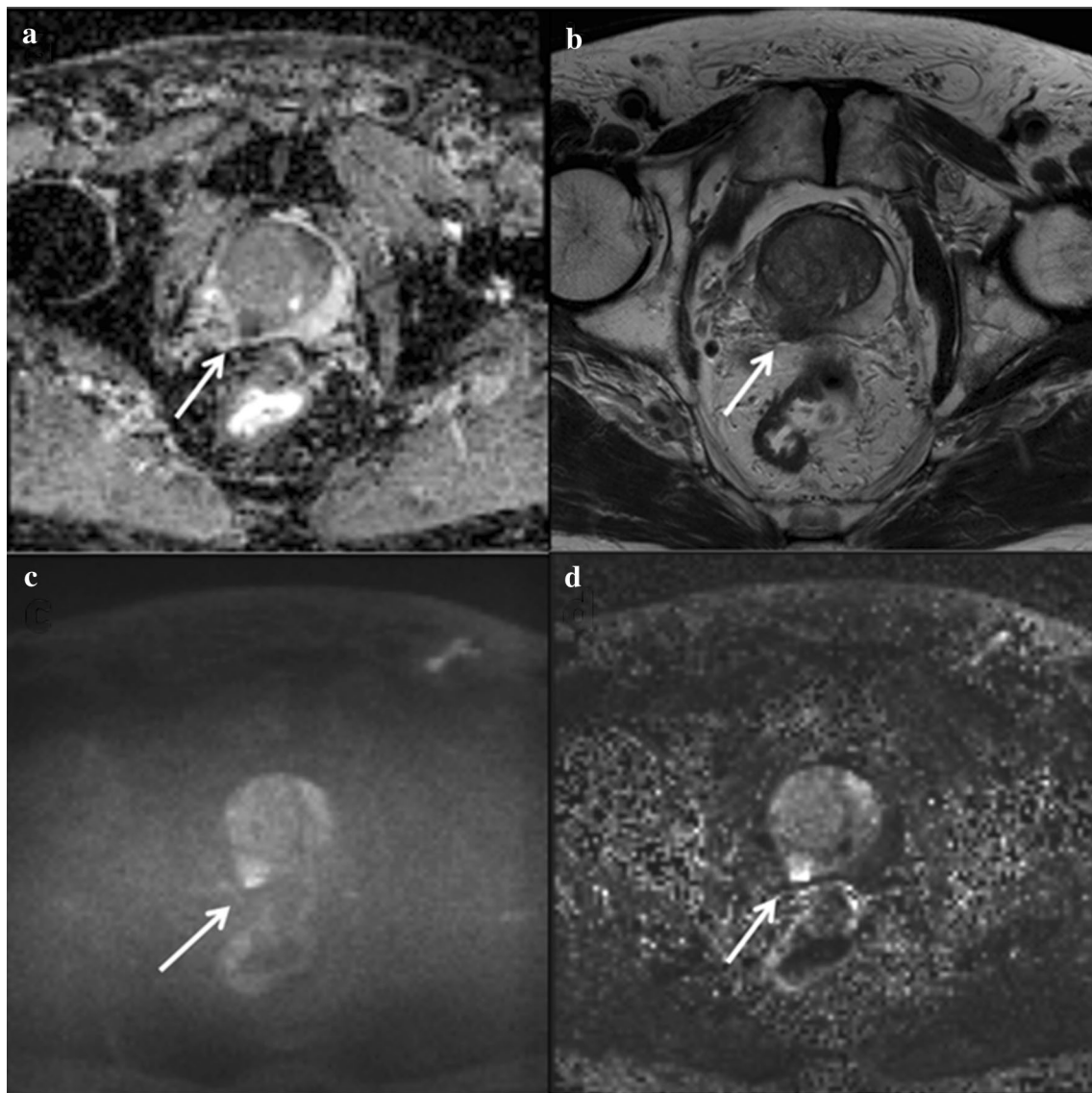
Fig. 3 A 81-year-old man with clinically significant prostate cancer (Gleason score 7 from biopsy, PSA = 17.85 ng/ml). Axial ADC (**a**) and T2-weighted image (**b**) demonstrate a focal lesion of low T2 signal and restricted diffusion. There is high signal within this lesion on acquired magnitude-averaged $b = 2000$ s/mm^2 image (**c**). The calculated $b = 2000$ s/mm^2 image (**d**) demonstrates comparable image quality for diagnostic evaluation. In addition, it provides better anatomic definition of the normal peripheral zone (seen as markedly hypointense signal). Better anatomic definition and improved lesion to background signal ratio might increase the diagnostic confidence for lesion detection

high b value (cHBV) images and found that these images are of noninferior image quality with comparable accuracy to acquired high b value images (aHBV) in detecting clinically significant prostate cancer. cHBV also provides comparable PIRADS score for histologically confirmed prostate cancer and may help in reducing the imaging time for prostate MRI (approx. 25% reduction in scan time).

Several prior studies have evaluated the cHBV images in prostate cancer with consistent results in terms of image quality and mixed results for the diagnostic accuracy [15, 17, 22]. Rosenkrantz et al. reported a superior image quality of cHBV compared to aHBV images with less image distortion but did not find any difference in the diagnostic accuracy between the two techniques [13]. Blackledge et al. reported that computed DW MR imaging in the body allows higher-b value images to be obtained with a good SNR and may improve disease detection [15]. Bittencourt et al. reported that a combination of a high b value extrapolation and sFOV may lead to increased diagnostic accuracy of DWI without an increase of acquisition time [22]. Grant et al., however, report that extrapolation using the IVIM model has equivalent lesion detection and similar image quality to acquired

Table 3 Comparing image qualities and levels of confidence between acquired and calculated high *b* value images

	Reviewer A	Reviewer B
Image quality		
Acquired complex-averaged high *b* value	2.67	2.69
Calculated complex-averaged high *b* value	2.70	2.64
P value*	0.34	0.52
Acquired magnitude-averaged high *b* value	1.81	2.10
Calculated magnitude-averaged high *b* value	1.92	2.25
P value*	0.10	0.07
Level of confidence		
Acquired complex-averaged high *b* value	4.10	4.37
Calculated complex-averaged high *b* value	4.24	4.35
P value*	0.20	0.43
Acquired magnitude-averaged high *b* value	3.01	4.06
Calculated magnitude-averaged high *b* value	3.32	4.10
P value*	0.02	0.38

*Mann–Whitney test was used for comparisons

DWI at $b = 1000$ s/mm^2 but is slightly inferior to acquired DWI at $b = 2000$ s/mm^2.

Our observations with the use of complex-averaging in DWI are unique and have never been studied before. As discussed in the Methods section, the magnitude-averaged DWI have a bias toward higher signal particularly in the image center, resulting in a haze-like background signal build-up. In adaptive combination of complex-valued images [18], a combination of images in local patches is performed without explicitly performing a phase correction of the single images. Thus, the averaged images are obtained that do not show a noise bias in the form of a background haze and which appear sharper. This may have resulted in the improvements of the image quality of aHBV images and potentially the increase in the diagnostic accuracy of

these images in this study. We used complex-averaging in combination with not only actual but also calculated HBV DW images. Both complex-averaging and calculated HBV images independently contributed in improvement in image quality and combination of the complex-averaging and calculated high *b* value resulted in highest image quality (Fig. 4) and diagnostic accuracy. Complex-averaging and cHBV images address different caveats of $b = 2000$ s/mm^2 images, such as background haze inherent to averaging and distortions and susceptibility effects. This might have resulted in synergistic effects that lead to highest quality and accuracy of complex-averaged cHBV images.

Limitations

This retrospective, single-center study has several limitations. Biopsy was the most common reference standard instead of prostatectomy which is susceptible to sampling errors. At our institution, 12 core biopsies are performed, and we subsequently matched the histopathology to the reported lesion on MRI through site descriptors (right vs left; base vs. mid-gland vs. apex). However, this does not completely eliminate bias. Also, decision to biopsy was made based on the results of subjective mp-MRI reads, and affecting actual diagnostic accuracy, which may be better than those reported.

Conclusion

The complex-averaging provides better IQ and LOC for DW images in prostate cancer without significant impact on ADC values. The cHBV images have the potential to replace aHBV and help in reducing the imaging time for prostate MRI. The complex-averaging when used in combination with cHBV may increase the accuracy for detection of the prostate lesions.

Table 4 Sensitivity, specificity, and accuracy for different datasets

Parameter	T2W, ADC, acquired DWI (conventional magnitude-averaged)		T2W, ADC, acquired DWI (complex-averaged)		T2W, ADC, calculated DWI (conventional magnitude-averaged)		T2W, ADC, calculated DWI (complex-averaged)	
	Value	95% CI	Value	95% CI	Value	95% CI	Value	95% CI
Sensitivity	63.1%	38.3–83.7%	73.6%	48.8–90.8%	63.1%	38.3–83.7%	68.4%	43.4–87.4%
Specificity	80%	59.3–93.1%	80%	59.3–93.1%	88%	68.7–97.4%	88%	68.7–97.4%
Accuracy	72.7%	57.2–85.04%	77.2%	62.1–88.5%	77.2%	62.1–88.5%	79.5%	64.7–90.2%
AUC	0.71	0.56–0.84	0.76	0.61–0.88	0.75	0.60–0.87	0.78	0.63–0.89

Fig. 4 Axial T2-weighted (**a**) and ADC images (**b**) demonstrate a focus of carcinoma with restricted diffusion. Acquired magnitude-averaged $b = 2000$ s/mm^2 image (**c**) demonstrates corresponding hyperintense signal. The application of complex-averaging results in improved signal-to-noise ratio and lesion conspicuity (**d**). Similarly, calculated high b value image results in better signal-to-noise ratio and lesion visibility (**e**), but, the combination of complex-averaging with calculated high b value (**f**) results in best image quality out of all 4 image sets. The PIRADS score assigned to this case was 3 based on the magnitude-averaged image (**c**) as it is mildly hyperintense. The score changed to 4 on complex-averaged calculated high b value image (**f**) where it appears markedly hyperintense. A 59-year-old man with clinically significant prostate cancer (Gleason score 7 from prostatectomy, PSA = 6.51 ng/ml)
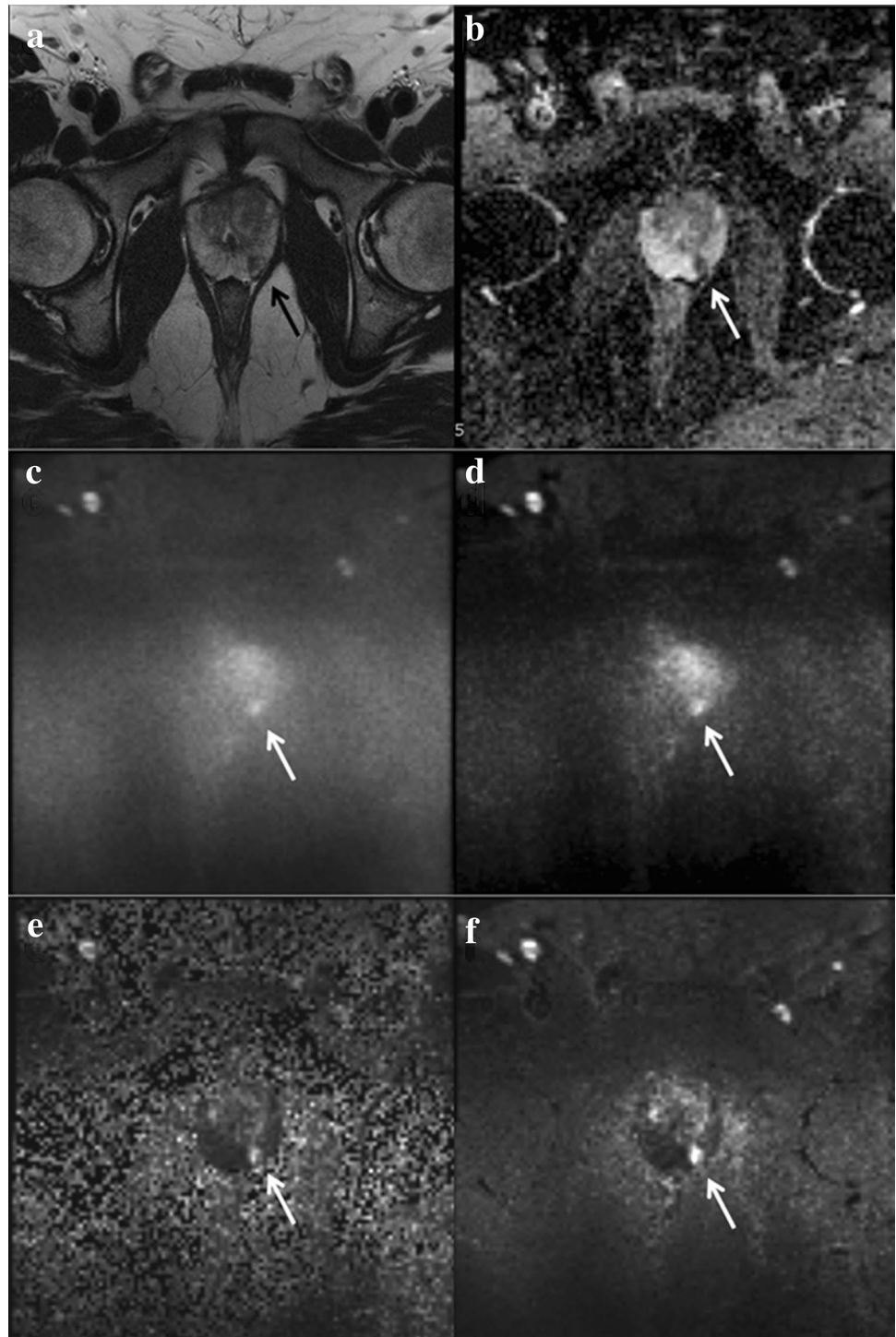
Compliance with ethical standards

References

1. Torre LA, Bray F, Siegel RL, Ferlay J, Lortet-Tieulent J, Jemal A. Global cancer statistics, 2012. CA Cancer J Clin. 2015 Mar 1;65(2):87–108.
2. Fütterer JJ, Briganti A, Visschere PD, Emberton M, Giannarini G, Kirkham A, et al. Can Clinically Significant Prostate Cancer Be Detected with Multiparametric Magnetic Resonance Imaging? A Systematic Review of the Literature. Eur Urol. 2015 Dec 1;68(6):1045–53.
3. Thoeny HC, Forstner R, De Keyzer F. Genitourinary Applications of Diffusion-weighted MR Imaging in the Pelvis. Radiology. 2012 May 1;263(2):326–42.
4. Baliyan V, Das CJ, Sharma S, Gupta AK. Diffusion-weighted imaging in urinary tract lesions. Clin Radiol. 2014 Aug 1;69(8):773–82.
5. Baliyan V, Das CJ, Sharma R, Gupta AK. Diffusion weighted imaging: Technique and applications. World J Radiol. 2016 Sep 28;8(9):785–98.
6. Kim CK, Park BK, Kim B. High-b-Value Diffusion-Weighted Imaging at 3 T to Detect Prostate Cancer: Comparisons Between b Values of 1,000 and 2,000 s/mm^2. Am J Roentgenol. 2010 Jan 1;194(1):W33–7.
7. Maurer MH, Heverhagen JT. Diffusion weighted imaging of the prostate—principles, application, and advances. Transl Androl Urol. 2017 Jun;6(3):490–8.
8. Grant KB, Agarwal HK, Shih JH, Bernardo M, Pang Y, Daar D, et al. Comparison of calculated and acquired high b value diffusion-weighted imaging in prostate cancer. Abdom Imaging. 2015 Mar;40(3):578–86.
9. Agarwal HK, Mertan FV, Sankineni S, Bernardo M, Senegas J, Keupp J, et al. Optimal high b-value for diffusion weighted MRI in diagnosing high risk prostate cancers in the peripheral zone. J Magn Reson Imaging. 2016 Jul 7;45(1):125–31.
10. Feng Q, Yan Y-Q, Zhu J, Tong J-L, Xu J-R. Optimal b value of diffusion-weighted imaging on a 3.0T magnetic resonance scanner in Crohn's disease. World J Gastroenterol WJG. 2014 Sep 21;20(35):12621–7.
11. Zhuang J, Lu Z-L, Vidal CB, Damasio H. Correction of eddy current distortions in high angular resolution diffusion imaging. J Magn Reson Imaging. 2013;37(6):1460–1467.
12. Shenoy-Bhangle A, Baliyan V, Kordbacheh H, Guimaraes AR, Kambadakone A. Diffusion weighted magnetic resonance imaging of liver: Principles, clinical applications and recent updates. World J Hepatol. 2017 Sep 18;9(26):1081–91.
13. Ogura A, Koyama D, Hayashi N, Hatano I, Osakabe K, Yamaguchi N. Optimal b Values for Generation of Computed High-b-Value DW Images. Am J Roentgenol. 2016 Jan 21;206(4):713–8.
14. Maas MC, Fütterer JJ, Scheenen TWJ. Quantitative evaluation of computed high B value diffusion-weighted magnetic resonance imaging of the prostate. Invest Radiol. 2013 Nov;48(11):779–86.
15. Rosenkrantz AB, Chandarana H, Hindman N, Deng F-M, Babb JS, Taneja SS, et al. Computed diffusion-weighted imaging of the prostate at 3 T: impact on image quality and tumour detection. Eur Radiol. 2013 Nov;23(11):3170–7.
16. Ueno Y, Takahashi S, Kitajima K, Kimura T, Aoki I, Kawakami F, et al. Computed diffusion-weighted imaging using 3-T magnetic resonance imaging for prostate cancer diagnosis. Eur Radiol. 2013 Dec;23(12):3509–16.
17. Blackledge MD, Leach MO, Collins DJ, Koh D-M. Computed diffusion-weighted MR imaging may improve tumor detection. Radiology. 2011 Nov;261(2):573–81.
18. Walsh DO, Gmitro AF, Marcellin MW. Adaptive reconstruction of phased array MR imagery. Magn Reson Med. 2000 May 1;43(5):682–90.
19. Garcia-Reyes K, Passoni NM, Palmeri ML, Kauffman CR, Choudhury KR, Polascik TJ, et al. Detection of prostate cancer with multiparametric MRI (mpMRI): effect of dedicated reader education on accuracy and confidence of index and anterior cancer diagnosis. Abdom Imaging. 2015 Jan;40(1):134–42.
20. Purysko AS, Rosenkrantz AB, Barentsz JO, Weinreb JC, Macura KJ. PI-RADS Version 2: A Pictorial Update. RadioGraphics. 2016 Jul 29;36(5):1354–72.
21. PIRADS-V2.pdf [Internet]. [cited 2019 Feb 9]. Available from: https://www.acr.org/-/media/ACR/Files/RADS/Pi-RADS/PIRADS-V2.pdf
22. Bittencourt LK, Attenberger UI, Lima D, Strecker R, de Oliveira A, Schoenberg SO, et al. Feasibility study of computed vs measured high b-value (1400 s/mm^2) diffusion-weighted MR images of the prostate. World J Radiol. 2014 Jun 28;6(6):374–80.

Affiliations

Hamed Kordbacheh[2] · Ravi Teja Seethamraju[5] · Elisabeth Weiland[3] · Berthold Kiefer[3] · Marcel Dominik Nickel[3] · Thitinan Chulroek[2,4] · Martina Cecconi[2] · Vinit Baliyan[2] · Mukesh G. Harisinghani[1,2]

Hamed Kordbacheh
hkordbacheh@mgh.harvard.edu

Ravi Teja Seethamraju
ravi.seethamraju@siemens-healthineers.com

Elisabeth Weiland
elisabeth.weiland@siemens-healthineers.com

Berthold Kiefer
berthold.kiefer@siemens-healthineers.com

Marcel Dominik Nickel
marcel.nickel@siemens-healthineers.com

Thitinan Chulroek
thitinan.c@chula.ac.th

Martina Cecconi
martinacecconi@hotmail.it

Vinit Baliyan
vbaliyan@mgh.harvard.edu

1   Harvard Medical School, Boston, USA

2   Department of Radiology, Massachusetts General Hospital,
    55 Fruit Street, White 270, Boston, MA 02114, USA

3   MR Applications Predevelopment, Siemens Healthcare
    GmbH, Erlangen, Germany

4   Department of Diagnostic Radiology, Faculty of Medicine,
    Chulalongkorn University and King Chulalongkorn
    Memorial Hospital, Bangkok, Thailand

5   MR Research and Technology, Siemens Medical Solutions
    USA, Inc, Boston, USA